Bub1 Up-Regulation and Hyperphosphorylation Promote Malignant Transformation in SV40 Tag–Induced Transgenic Mouse Models

Conghui Guo,[1] Guojun Wu,[1] Joseph L. Chin,[1,3] Glenn Bauman,[3] Madeleine Moussa,[2] Feng Wang,[4] Norman M. Greenberg,[5] Stephen S. Taylor,[6] and Jim W. Xuan[1,2]

Departments of [1]Surgery, [2]Pathology, and [3]Oncology, University of Western Ontario, London, Ontario, Canada; [4]Institute of Biosciences and Technology, Texas A&M University System Health Science Center, Houston, Texas; [5]Clinical Research Division, Fred Hutchinson Cancer Research Center, Seattle, Washington; and [6]School of Biological Sciences, University of Manchester, Manchester, United Kingdom

Abstract

Rodents do not naturally develop prostate cancer. Currently, most widely used genetically engineered mouse prostate cancer models use SV40 T/tag oncogene. To understand the mechanism underlying prostate cancer development in transgenic and knock-in SV40 Tag mouse models, we did cDNA microarray analyses, comparing gene expression profiles of prostate cancer tissues from early-, late-, and advance-stage androgen-independent prostate cancers. Of the 67 genes that were up-regulated by ≥10-fold, 40 are known to be required for chromosome stability. In particular, the spindle checkpoint component Bub1 was persistently up-regulated from early to advanced androgen-independent prostate cancer lesions. Significantly, Bub1, which is required for accurate chromosome segregation during mitosis, has recently been reported to bind SV40 Tag. Consistent with a spindle checkpoint defect, flow cytometry experiments indicate that advanced androgen-independent prostate cancer tumors exhibit aneuploidy, along with up-regulation of levels of both Bub1 mRNA and Bub1 protein or hyperphosphorylation. Importantly, up-regulation and hyperphosphorylation of Bub1 were also observed in established human prostate cancer cell lines and in clinical studies. Furthermore, analysis of human prostate cancer lines showed impaired spindle checkpoint function and endoreduplication following exposure to spindle toxins. Small interfering RNA–mediated repression of Bub1 in the human prostate cancer line PC-3 restrained cell proliferation, an effect mimicked by inhibition of mitogen-activated protein kinase, an upstream activator of Bub1. Thus, by perturbing Bub1 function, our observations suggest a new mechanism whereby the SV40 Tag oncoprotein promotes chromosomal instability and aneuploidy in transgenic mouse prostate cancer models. Whereas the exact details of this mechanism remain unclear, our novel findings raise the possibility of exploiting Bub1 as a new therapeutic target in the treatment of prostate cancer, the most common cancer in adult men in North America.
(Mol Cancer Res 2006;4(12):957–69)

Introduction

Prostate cancer is the most frequently diagnosed malignancy among adult males in North American. Because prostate cancer does not occur naturally in rodents, current basic and preclinical trial studies on prostate cancer use genetically engineered mouse models. Both transgenic and knockout techniques using prostate tissue–specific promoters were adopted in an attempt to model the human clinical situation in all aspects (for reviews, see refs. 1, 2). The SV40 T/t antigen (Tag) oncogene–derived transgenic prostate cancer mouse models, the rat probasin gene–based transgenic adenocarcinoma mouse prostate (TRAMP; refs. 3-5) and LPB-SV40 tag (LADY; ref. 6) models, are currently the most prevalent murine prostate cancer model. All SV40 Tag–derived autochthonous genetically engineered models develop tumor spontaneously in a genetically defined and immunocompetent background. The TRAMP model shows salient characteristics of human prostate cancer, progressing from mouse prostatic intraepithelial neoplasia to prostate cancer by 12 weeks, then to advanced and highly invasive metastatic cancer. The cancer progresses from an androgen hormone–dependent to a hormone-independent and -resistant disease. Other SV40 Tag models were C3 (1) SV40 T, Cryptdin-2 SV40 T, Fetal Gγ-globin, and PSP94 SV40 T/t (reviewed in refs. 1, 2, 7, 8).

SV40 Tag is a powerful oncoprotein capable of transforming a variety of cell types by introducing karyotypic instability (for review, see refs. 9-12). The ability of T antigen to cause karyotypic instability in human cells has been found to correlate with its ability to deregulate normal mitotic checkpoints, but the exact mechanism is not known. The transforming activity of

Received 6/19/06; revised 9/28/06; accepted 9/28/06.
Grant support: Canadian Institute of Health Research grants MOP-77684 and UOP-63722, Prostate Cancer Research Foundation of Canada (J.W. Xuan) and NIH-National Cancer Institute grant 2 U01 CA084296-06 (N.M. Greenberg and J.W. Xuan).
The costs of publication of this article were defrayed in part by the payment of page charges. This article must therefore be hereby marked advertisement in accordance with 18 U.S.C. Section 1734 solely to indicate this fact.
Note: Supplementary data for this article are available at Molecular Cancer Research Online (http://mcr.aacrjournals.org/).
Requests for reprints: Jim W. Xuan, Urology Research Laboratory, London Health Sciences Centre, 375 South Street, London, Ontario, Canada N6A 4G5. Phone: 519-667-6682; Fax: 519-432-7367. E-mail: jim.xuan@lhsc.on.ca

doi:10.1158/1541-7786.MCR-06-0168

Tag is largely due to its perturbation of the retinoblastoma (pRB) and p53 tumor suppressor proteins. Tag provides ATPase and DNA helicase activities, as well as DNA binding activity. In addition, Tag binds to several other cellular factors, including the transcriptional coactivators p400, p107, p300/CBP, p130/pRB2, etc. (reviewed in refs. 9-12). A recent report on yeast two-hybridization and immunoprecipitation techniques showed that the *Bub1* gene is another targeting protein of SV40 Tag (9).

Table 1. List of Highly Up-Regulated (>10-Fold) Genes in KIMAP Prostate Cancer Models Higher than Normal as Shown by cDNA Microarray

Gene symbol	Gene description	20 wk	60 wk
Genes related to chromosome instability			
Group 1: DNA damage checkpoint (G_1 and G_2)			
Brca1	Breast ovarian cancer susceptibility homologue	58.55	66.2
Chk1	Checkpoint kinase 1 homologue (*Schizosaccharomyces pombe*)	40.49	47.1
Rad541	RAD54 like (*Saccharomyces cerevisiae*)	28.86	30.0
Mbd4	Methyl-CpG binding protein MBD4	26.15	28.5
Rad51ap1	RAD51-associated protein 1	24.65	41.3
Taac3	Transforming, acidic coiled coil–containing protein 3	24.63	15.3
E2f1	E2F transcription factor 1	13.67	16.4
Pole	DNA polymerase ϵ	11.67	13.5
Oasl2	2-5 oligoadenylate synthetase-like 2	10.83	15.4
Group 2: replication checkpoint			
Cyclin B2	Cyclin B	87.82	69.8
Cyclin B	Cyclin B	71.14	38.6
Rep 3	Similar to replication factor C (activator 1) 3	40.44	36.6
mcmd5	Minichromosome maintenance deficient 5	26.22	17.9
Hcapg	Chromosome condensation protein G	24.1	28.5
Skp2	S-phase kinase-associated protein 2	21.57	20.3
Mcmd/Mcm3	Minichromosome maintenance deficient	19.43	12.6
cdc6	Cell division cycle 6	17.22	14.9
mcmd6	Minichromosome maintenance deficient 5	15.49	19.1
ccnf	Cyclin F	15.17	13.0
Eif4a2/repC	Eukaryotic translation initiation factor 4A2	11.98	14.7
Prc1	Protein regulator of cytokinesis 1	11.66	6.79
Cdc45l	Cell division cycle 45	11.63	7.79
Cdc2a	Cell division cycle 2 homologue A	11.18	7.59
Group 3: spindle checkpoint			
Bub1	Mitotic checkpoint protein kinase	60.09	37.3
Arc1	Activity-regulated cytoskeletal-associated protein	35.1	2.08
Diap3	Diaphanous homologue 3	27.15	27.3
Ube2c	Ubiquitin-conjugating enzyme E2C	23.2	15.8
Bub1b	Budding uninhibited by benzimidazoles 1 homologue, β	20.98	17.1
pttg/securin	Pituitary tumor transforming gene protein	17.68	14.9
Klf6/Kif22	Microtubule-associated motor KIF4	15.48	17.8
Rab6kif1	Kinesin-like (Rab6kifl)	15.37	19.3
spag5	Sperm-associated antigen 5	14.71	15.5
Ranbp17	RAN binding protein 17	14.19	10.5
Np95	Nuclear protein 95	13.46	18.9
H2afx/Kif 2	H2A histone family, member X	13.37	9.59
Pim	Proviral integration site 1	12.83	18.33
RHAMMV5	Hyaluronan receptor RHAMMV5	11.86	10.69
Hmg 2	High-mobility group 2 protein	11.49	13.22
Sox 4	SRY-box containing gene 4	11.49	12.58
Usp 18	Ubiquitin-specific protease 18	10.76	11.42
Genes related to apoptosis			
FN14	Type I transmembrane protein	101.4	50.37
cd27	Cd27 binding protein (Hindu God of destruction)	50.23	46.79
Ki67		24.59	20.45
Traf 4	Tnf receptor-associated factor 4	18.84	18.49
Other effector kinase, oncogenes			
Racgap1	Rac GTPase-activating protein 1	188.12	130.32
Mel K	Maternal embryonic leucine zipper kinase	54.12	75.41
EGF-BP	Kallikrein 9	38.84	33.48
Gzmd	Granzyme D	33.89	891.09
Egr1	Early-growth response 1	27.36	10.18
Ttk	Ttk protein kinase	22.79	15.93
ect 2	ect2 oncogene	18.72	14.46
Pglyrp	Peptidoglycan recognition protein	16.94	30.44
Fos	FBJ osteosarcoma oncogene	15.73	6.55
G7e	G7e protein	13.59	15.03
Tmprss4	Transmembrane protease, Ser^4	13.21	16.32
Slc25a19	Solute carrier family 25, member 19	13.11	6.89
Vig1	Hemorrhagic septicemia virus (VHSV) induced gene 1	11.21	4.84
Pbk	T cell–originated protein kinase/PDZ binding kinase	10.82	7.13
Siat7b	Sialyltransferase 7	10.29	3.41

(Continued on the following page)

Table 1. List of Highly Up-Regulated (>10-Fold) Genes in KIMAP Prostate Cancer Models Higher than Normal as Shown by cDNA Microarray (Cont'd)

Gene symbol	Gene description	20 wk	60 wk
Genes related to immunoresponse			
MCP-5	Monocyte chemoattractant protein-5 precursor	19.11	28.19
IL18BP	Interleukin-18 binding protein d precursor	14.43	23.04
Defcr3	Defensin-related cryptdin 3	14.25	12.61
Igl-V1	Immunoglobulin λ chain, variable 1	10.81	77.64
Scyb10	Cytokine B subfamily (Cys-X-Cys), member 10 (Scyb10)	10.15	5.66
Genes related to the prostate function			
GK21	Glandular kallikrein 2	50.19	27.04
Ccsg2	Germ cell-specific gene 2	16.43	11.74
Klk27	Kallikrein 27	17.29	9.01

There seems to be ample evidence that other factors contributing to the transformation potential of SV40 Tag are yet to be fully elucidated. The ability of T antigen to deregulate cell proliferation depends on its specific interaction with a variety of host cell proteins, studies of which have led to the elucidation of many different signaling pathways in different cancer modeling systems (12-18).

Prostate cancer has proved to be a complicated disease due to its heterogeneous and multifocal nature (2, 7). The stochastic and nonsynchronous incidence in transgenic prostate cancer mice is a prominent feature of TRAMP and most other SV40 Tag–derived mouse models. We have constructed two mouse models of *PSP94* (prostate secretory protein of 94 amino acids) gene–directed transgenic (PSP-TGMAP) and knock-in (PSP-KIMAP) adenocarcinoma of the prostate using the SV40 T/tag oncogene. PSP94 (also named β-microseminoprotein) is one of the three most abundantly secreted proteins from the prostate gland (the others being prostatic acid phosphatase and prostate-specific antigen; refs. 19, 20). Mouse *PSP94* gene expression is very prostate tissue specific, as shown in our transgenic prostate cancer models, because no tumors in other tissues [e.g. reportedly expressing PSP94 (mucous tissues such as in gastric, trachea, and bronchi; refs. 21, 22)] have ever been identified (4, 23, 24). The PSP94-TGMAP model showed similarities to the most commonly used TRAMP model (3, 4), including spatial (prostate tissue) and temporal (after puberty) specificity of tumor induction, rapid tumor growth, histopathologic grading, androgen dependence, and responsive and eventual androgen refractoriness in hormone deprivation therapy (4, 23, 24), as shown by our newly developed technology of three-dimensional ultrasound imaging (5) and a mouse serum PSP94 biomarker (25). The PSP-KIMAP model has features similar to human prostate cancer, including protracted prostate cancer development kinetics of the majority of well-differentiated to moderately differentiated prostate cancer, tumor heterogeneity, and multifocality (23-25). Prostate cancer development in KIMAP is highly predictive, synchronous, and with highly stable phenotypes and genotypes.

Because there have been few systematic studies on global gene profiling of the SV40 Tag–derived mouse transgenic prostate cancer models, we took advantage of the synchronous and protracted prostate cancer growth feature of our knock-in SV40 Tag mouse model and did a series of chip assays. We found that the up-regulation of genes related to checkpoint systems is the major feature in both transgenic and knock-in SV40 Tag–derived mouse prostate cancer models, with different levels of hyperphosphorylation. Among those mitotic checkpoint genes, we further identified a new mechanism whereby the *Bub1* gene plays a key role in tumorigenesis and progression toward advanced androgen-independent prostate cancer.

Results

Checkpoint Genes Related to Chromosome Instability and Aneuploidy Are the Most Differentially Expressed Genes in SV40 Tag–Derived Mouse Prostate Cancer Models

To study global gene profiles of SV40 Tag oncogene in mouse prostate cancer models, cDNA microarray was done. We used a newly established knock-in SV40 Tag model (KIMAP; refs. 23, 24) for studying the mechanism of tumorigenesis and progression, as the transgenic prostate cancer growth in KIMAP mice is synchronous, with long and protracted well-differentiated to moderately differentiated prostate cancer from early stage (20 weeks of age, $n = 7$; with mouse prostatic intraepithelial neoplasia, microinvasion, and well-differentiated to moderately differentiated prostate cancer) to the late stage (60 weeks, $n = 10$; moderately to poorly differentiated prostate cancer) developments.

Table 1 summarizes the results of cDNA microarray analysis. Only genes up-regulated ≥10-fold (than wide type) were listed and classified. The majority (40 of 67) of these highly expressed genes (total of 67 genes) that are related to chromosome instability. Three subgroups were further categorized, although with some overlapping functions: DNA damage checkpoint (10 of 67), replication checkpoint (13 of 67), and mitosis checkpoint (17 of 67; mostly belonging to the spindle checkpoint group). Most of these genes were constantly up-regulated from 20 to 60 weeks of prostate cancer development in KIMAP mice.

Several lines of evidence of the authenticity and reliability of cDNA microarray are (*a*) both PSP94 and rPB gene expressions were down-regulated by 30- and 50-fold (see Supplementary Table S1), as expected. (*b*) Bub1, a SV40 Tag oncogene interaction protein (9), was up-regulated. (*c*) The following same gene, or similar genes, were repeatedly identified in the test: *FN14* (thrice), *Mcmd5* and *Mcmd6* (four times), *Taac* (twice), and *Kinesin* (*Klf4* and *Klf6*; twice); some

unknown genes with similar putative functions were repeatedly found as well (data not shown). (*d*) Prostate tissue–specific or prostate function–related genes changed as expected with tumorigenesis: PSP94, rPB, male-specific protein cytochrome *P*450 (100-fold down-regulated), GK21 (glandular kallikrein; 50-fold up-regulated), Klk27 (kallikrein 27; 17.29-fold up-regulated), and Ccsg2 (germ cell–specific gene 2; 16-fold up-regulated). (*e*) Immunoresponse genes were repeatedly confirmed, with the same results between transgenic and KIMAP models as reported previously (24).

None of the checkpoint gene groups were found in the list of down-regulated genes. In the list of 10- to 20-fold down-regulated genes (n = 71; see Supplementary Table S1), most were related to loss of normal prostate function, such as secretion of PSP94, rPB, cytochrome *P*450 (male-specific steroid induced 3a11), major urinary proteins (mup1 and mup3), and apolipoprotein. The list also includes several proteinase inhibitors such as serpins (b7, b1, b5, c1, f2, e2) and hepsin. Genes related to cell matrix changes, such as fibrogen and sialoprotein, were also significantly down-regulated.

To further verify the cDNA microarray results, a semiquantitative reverse transcription-PCR (RT-PCR) reaction on the RNA pools for the chip assay in KIMAP mice was done (Fig. 1A). Consistent with cDNA microarray, there was an up-regulation of mRNA of Bub1 and Bub1b (BubR1), with *GAPDH* as internal reference. The same results were obtained with BubR1 as Bub1 (Fig. 1A). Prostate cancer samples from TGMAP mice were also tested and the RT-PCR signals (25 cycles) of Bub1 are higher than those of KIMAP mice. The up-regulation of those checkpoint genes presents both in cytoplasmic and nuclear RNAs (data not shown).

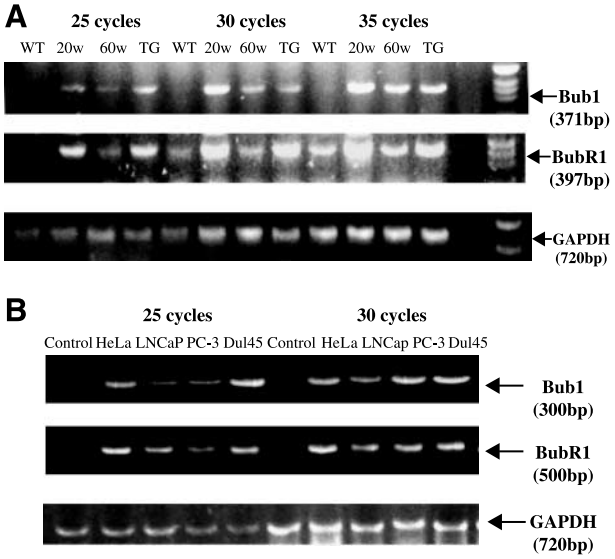

FIGURE 1. Semiquantitative RT-PCR analyses of the pooled (n = 12) total RNA extracted from TGMAP (*TG*) and KIMAP (*KI*) mice and human prostate cancer cell lines for verification of results of cDNA microarray experiments. Total RNA samples were normalized by the control gene *GAPDH* (*first row, 720 bp*). Numbers indicate the number of thermocycles of each PCR amplification. **A.** Bub1 and BubR1 in TGMAP (*TG*), KIMAP, and normal (*WT*) mouse prostate tissues. KIMAP mice were from 20 wk (*20w*) to 60 wk (*60w*) of age. **B.** Bub1 and BubR1 mRNA levels in three human prostate cancer cell lines, LNCaP, PC-3, and DU145. HeLa cells and human normal prostate tissues were used as controls.

Because there has been no report on the two checkpoint genes *Bub1* and *BubR1* in human prostate cancer cell lines, we also assessed if the increased mRNA levels of Bub1 and BubR1 was present in three human prostate cancer cells [two androgen independent (DU145 and PC-3) and one androgen dependent (LNCaP)]. Stronger RT-PCR signals of Bub1 and BubR1 were detected in LNCaP, PC-3, and DU145, whereas LNCaP cell showed less Bub1 mRNA (Fig. 1B). Adjacent normal prostate tissues (histologically confirmed) from patients with prostate cancer were used as control, in which there was not any signal in the gel (Fig. 1B).

A Comparative Study of Chromosome Ploidy by Flow Cytometry and SV40 Interacting Proteins in TGMAP and KIMAP Mice and Human Prostate Cancer Cell Lines

To show if the up-regulation of checkpoint genes in prostate cancer in both KIMAP and TGMAP mice is associated with the chromosomal aneuploidy, flow cytometry experiments were done. Only visible tumor samples of both KIMAP and TGMAP from late-stage prostate cancer were tested. TGMAP tumor tissue (prostate tumor weight, 2-15 g/mouse) was collected showing the majority of androgen-independent and neuroendocrine carcinoma (4, 5, 23, 24). Diploid control tissue samples were from normal spleen cells or peripheral blood leukocytes (Fig. 2A). All eight TGMAP tumors revealed typical aneuploid changes as shown in Fig. 2B. In the eight KIMAP tumor samples analyzed, seven mice showed mostly a diploid tumor peak (89%; Fig. 2C) and only one mouse revealed a tetraploid peak (11%; Fig. 2D), which is similar to the reported clinical distribution (75% diploid and 25% nondiploid tumor; ref. 26; Table 2). We showed that the advanced prostate cancers (androgen independent and neuroendocrine; refs. 4, 5) in our TGMAP model were different from most of the clinical prostate cancer samples (26) with a higher incidence of aneuploidy.

Because three human prostate cancer cell lines also showed up-regulation of Bub1 and BubR1 mRNA, flow cytometry experiments were also done to assess the correlation with chromosome ploidy. As shown in Table 2, these three human prostate cancer cell lines showed similar flow cytometry patterns, with TGMAP mostly with aneuploid structure (3N and 4N).

Using flow cytometric analysis, the higher DNA proliferation rates (as determined by %S and %S + $\%G_2$-M) of advanced prostate cancer from TGMAP mice were identified. The average figures were 7.1% and 49.7%, respectively, indicating a higher chromosomal proliferation rate associated with rapid tumor growth in TGMAP mice. Two androgen-independent human prostate cancer cell lines (PC-3 and DU145) showed higher chromosome proliferation rates, close to that of TGMAP (Table 2), whereas KIMAP mice had %S and %S + $\%G_2$-M values of 3.6% and 10.7%, respectively, which is close to the clinical incidence of 3.1% and 10.5%, respectively (refs. 24, 26; Table 2).

To differentiate between gene profiles of TGMAP and KIMAP models, a second set of cDNA microarray was done (n = 12 mice). The fast-growing transgenic prostate cancers (PSP-TGMAP), all with palpable tumors with androgen-independent and neuroendocrine features (average, 3-15 g/35 g of body weight), were used as advanced prostate cancer, the

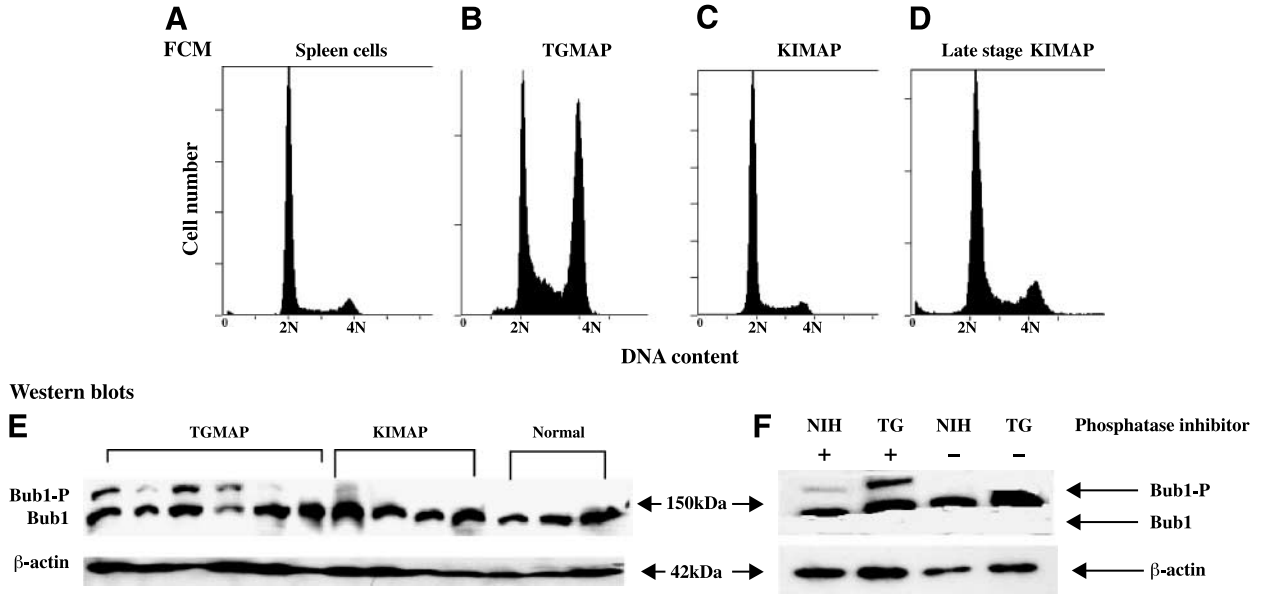

FIGURE 2. Flow cytometry (**A-D**) and Western blotting (**E-F**) experiments showing that chromosomal aneuploidy is accompanied by hyperphosphorylation of Bub1 protein in transgenic prostate cancer samples from TGMAP and KIMAP models. **A** to **D.** Flow cytometry analyses of late-stage prostate cancer samples from both TGMAP and KIMAP models. All diagrams are singlet pictures, with cell counts (*Y-axis*) plotted against PI int (propidium iodide). The first peak C (cell cycle phase G_0-G_1) is for diploid, peak D (S phase) is for aneuploid cells, and peak E (G_2-M phase) for tetraploid separately. **A.** Normal spleen tissue dissociated cells from KIMAP mice (control for diploid). **B.** Mixture of prostate cancer cells of TGMAP mice showing aneuploidy with spleen cells (as internal control). **C.** Prostate cancer cells of KIMAP mice showing diploidy. **D.** Prostate cancer cells of KIMAP mice showing tetraploid changes. **E** and **F.** Western blot showing the hyperphosphorylation (**E**; *Bub1-P*) of Bub1 protein in most of TGMAP mice tumors and in one KIMAP tumor sample. **F.** Western blot showing the detection of the Bub1 phosphorylated forms (*Bub1-P*; 150 kDa as recommended by the manufacturer). Samples from NIH 3T3 mouse cells and TGMAP tumors were treated with or without phosphatase inhibitor. All Western blots were normalized semiquantitatively by internal reference β-actin to show equal loading of tissue lysate proteins.

most differentiated genes being neuroendocrine-related genes as we have reported (5, 24). Prostate cancer tissue from the KIMAP model revealed features of slow-growing and moderately differentiated (androgen dependent) prostate cancer. SV40 Tag targeting and interacting/binding proteins (either direct or indirect) and checkpoint system genes were compared by the chip test between the two models of TGMAP and KIMAP. Only the *Bub1* gene was up-regulated among all reported SV40 Tag interaction proteins. Other SV40 Tag targeting genes (10, 11), either direct or indirect (p53, pRb, p300/CBP, p107, p130, p400, Nbs (DNA repair), Fbxw7, etc.) were all less significantly up-regulated in either KIMAP or TGMAP models (listed in detail in Supplementary Table S2), indicating a specific role of Bub1 up-regulation in transgenic prostate cancer models. Compared with *Bub1* gene, other checkpoint system genes, including those involved in kinetochore, cell cycle regulation, and mitosis and some kinase related to cell division, are also less up-regulated in both TGMAP and KIMAP models [e.g., mitogen-activated protein kinase (*MAPK*), *Skp2, Plk, Mad2, Cenp-H, APC/C5*, etc.; Supplementary Table S2].

Table 2. Comparison of DNA Ploidy and Proliferation in KIMAP and TGMAP Models and Human Prostate Cancer Cell Lines

	TGMAP	KIMAP	Clinic[35]	LNCaP	PC-3	DU145	PBL
DNA ploidy by flow cytometry							
Diploid (%)	0	89	75	0	0	0	100
Nondiploid (%)	100	11	25	100	100	100	0
Triploid					100	100	
Tetraploid	100	11	25	100			
Aneuploid	100			100	100	100	
DNA proliferation by flow cytometry							
%S	17.3	3.6	3.1	5.54	17.5	19.1	1.9
%S + %G_2-M	23	10.7	10.5	12.1	326	35.1	2.42

Abbreviations: %S, percent S phase; %S + %G_2-M, percent S phase and G_2-M phase; PBL, peripheral blood leukocytes.

Bub1 Protein Up-Regulation in Hyperphosphorylated Forms in Late Stages of Transgenic Prostate Cancer in SV40 Tag–Induced TGMAP and KIMAP Models

Because mitotic checkpoint *Bub1* gene expression is the only cell cycle– and mitosis-related gene highly up-regulated at the mRNA level in either KIMAP (early and late stage) or TGMAP mice (advanced stage, androgen independent and neuroendocrine), we assessed the protein expression of Bub1 in transgenic prostate cancer models by Western blotting experiments. Figure 2E showed Western blot results of transgenic prostate cancer tumor samples from TGMAP (n = 8) and KIMAP (n = 5) models compared with normal mouse prostate tissue (n = 5). The nonactive form of Bub1 protein was found to be not significantly changed (Fig. 2F). However, in almost all of the TGMAP sample lysates, high levels of phosphorylation bands (Bub1-P) were shown with the upper band (119.5 kDa; apparent molecular weight, 150 kDa) undergoing a mobility shift in Western blots (Fig. 2F), whereas only one of six KIMAP tumors showed a faint phosphorylation band. To

confirm that this mobility shift band is phosphorylated Bub1, its sensitivity to phosphatase was tested. Lysates with and without added phosphatase inhibitor were tested as positive and negative controls, separately (Fig. 2F). Synchronized and nocodazole-treated mouse NIH 3T3 cells were used as controls, and β-actin signals in the Western gel were used as normalizing internal references.

Hyperphosphorylation of Bub1 Protein Is Associated with Impaired Spindle Checkpoint Function and Chromosomal Endoreduplication

Because human prostate cancer cell lines revealed similar aneuploidy changes as in poorly differentiated, advanced, androgen-independent and neuroendocrine prostate cancer in TGMAP, and because they also revealed up-regulated Bub1 mRNA expression, we tested if Bub1 hyperphosphorylation was also present in those cell lines. To evaluate the effect of phosphorylation of Bub1 on mitosis, DNA ploidy and mitotic index were also monitored and determined simultaneously. HeLa cells were used as a control for mitotic checkpoint arrest with nocodazole (microtubule toxin) treatment.

As shown in Fig. 3A, Western blot analysis indicated that Bub1 protein level was very low or not detectable in normal mouse prostate tissue and in asynchronously growing PC-3, DU145, and HeLa cells, whereas it was detectable in the synchronized cells at the G_1-S phase boundary using a double thymidine block (Fig. 3A) and lasted for 48 h in the synchronized cells (Fig. 3B). However, no phosphorylation band was detected (Fig. 3B).

Next, to interfere with the spindle body assembly, nocodazole was added to both synchronously growing HeLa and PC-3 cells after release from G_1-S. Figure 3C shows that HeLa cells responded to nocodazole treatment with a peak of Bub1 phosphorylation at 12 h, then diminishing after 24 h. Mitotic arrest was completed 24 to 30 h later. Figure 3D shows the cell morphology, with dead HeLa cell visible 48 h after nocodazole treatment. As shown in Fig. 3C, PC-3 showed a peak of Bub1 phosphorylation 12 h after nocodazole treatment. However, PC-3 cells were different from HeLa cells, as a weak Bub1 phosphorylation band (Bub1-P) was still detectable up to 42 h. BubR1 showed a similar hyperphosphorylation band (BubR1-P, Fig. 3C). Both Bub1 and BubR1 showed delayed, incomplete mitotic arrest and persistent hyperphosphorylation in the presence of nocodazole. Increased cell death in PC-3 was not seen 48 h after nocodazole treatment. Figure 3E also shows that HeLa cells had a standard mitotic arrest peak 12 to 18 h after nocodazole-induced mitotic arrest, whereas no mitotic arrest peak and lower mitotic index were found in the PC-3 cell line, indicating less responsiveness of PC-3 cells to nocodazole treatment.

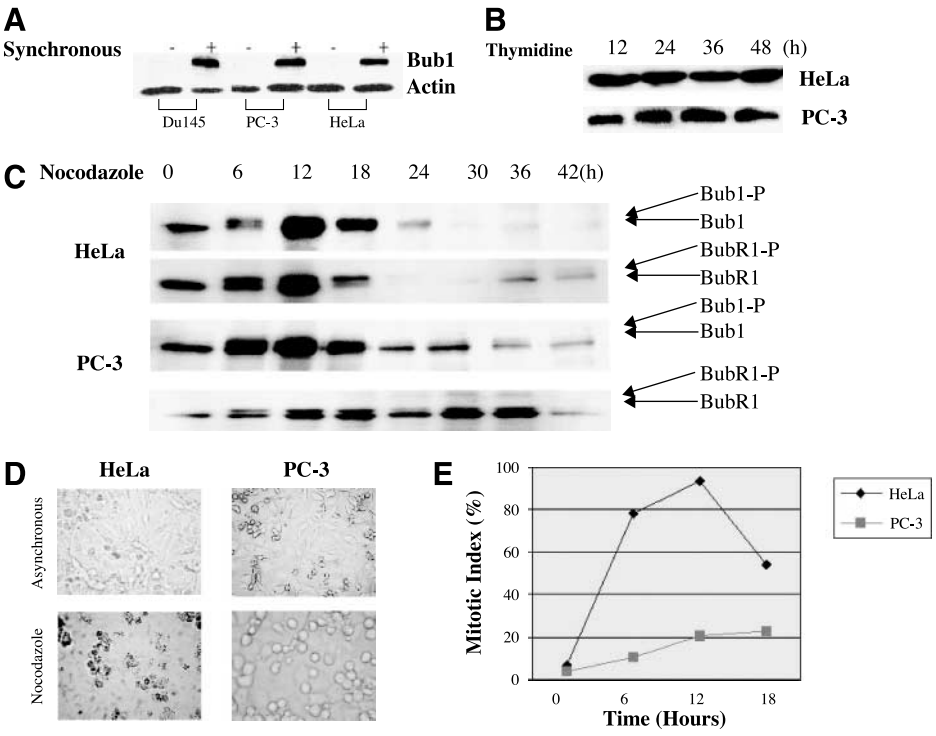

FIGURE 3. Western blot showing hyperphosphorylation of Bub1 protein in human PC-3 prostate cancer cell lines in synchronously growing cells treated with microtubule-disrupting agent nocodazole. **A.** Western blot detection of Bub1 protein in synchronous and asynchronous PC-3, DU145, and HeLa cells with (+) or without (−) double thymidine treatment. **B.** Western blot detection of Bub1 protein in synchronously growing PC-3 and HeLa cells at a time course of 12 to 48 h of double thymidine treatments. **C.** Western blots showing time course analyses of HeLa and PC-3 cells with synchronous growth and nocodazole treatments. Hours (0-42 h) of times course exposed to nocodazole were indicated. Both Bub1 and BubR1 proteins and their phosphorylated forms (*Bub1-P* and *BubR1-P*) were discernible by arrows in 10% SDS-PAGE. **D.** Morphology of synchronously growing HeLa and PC-3 cells treated with nocodazole. Pictures were taken under an invert microscope. Magnification, ×10. **E.** Graphical comparison of the time course of mitotic index of HeLa and PC-3 cells after nocodazole treatment in synchronously growing cells, showing different responses of mitotic arrest.

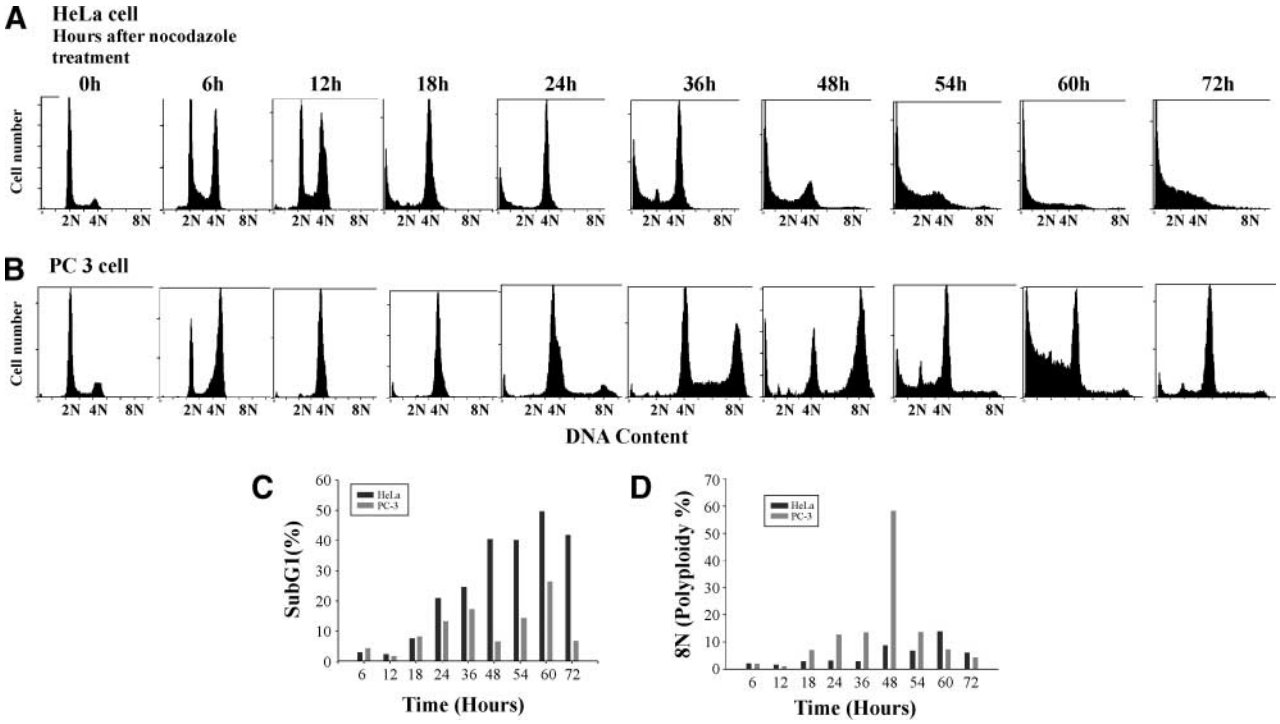

FIGURE 4. DNA content analyses by flow cytometry with the time course of synchronous growth cells of HeLa (**A**) and human prostate cancer PC-3 cells (**B**) exposed to nocodazole. **C.** Bar graph derived from **A** and **B** showing the accumulation of sub-G_1 cells (<2N; shown by relative percentages), possibly undergoing apoptosis and cell death in HeLa and PC-3 cell lines. **D.** Bar graph derived from **A** and **B** showing the accumulation of percentages of polyploidy (8N) cell populations in HeLa and PC-3 cells, showing chromosomal overproliferation and cytokinesis.

To study the effect of the abnormal mitotic checkpoint function (not complete mitotic arrest) on chromosomal ploidy in human PC-3 cells, flow cytometry was done to determine DNA content in the time course of nocodazole treatment of synchronously growing PC-3 cells. HeLa cells were used as a control.

Results were shown in Fig. 4A and B. From the first 24 h after release from G_1-S, both populations (HeLa and PC-3) progressed through S phase and entered G_2 and M phases with similar kinetics (Fig. 4A and B), with a DNA content of 4N. However, HeLa cells showed an increased mitotic index (4N peak in DNA content), indicating mitotic arrest (Fig. 3E). PC-3 cells showed a lower mitotic index than HeLa cells, without a significant mitotic arrest peak (Fig. 3E). This result is very similar to the arrest failure of lung cancer cell lines (27). PC-3 cells progressed through S phase and entered G_2, with continued chromosomal endoreduplication, with DNA content increasing from 4N to 8N as shown by flow cytometry (Fig. 4A). After 54-h nocodazole treatment, PC-3 cells maintained their tetraploidy.

HeLa cells showed only transient arrest for 48 h before cell death (Figs. 3D and 4A), possibly undergoing apoptosis. The PC-3 cell population after 48 h showed continued chromosome endoreduplication, cell cycle progression, and accumulation DNA content to 4N (Fig. 4B). By 48 h, the majority of these cells completed S phase, producing a large population of cells with 8N DNA content (Fig. 4B and D). By 54 h, these cells entered a second mitosis cycle, with DNA content of 4N, indicating continuous chromosomal segregation and cytokinesis (Fig. 4B). As shown in Fig. 3D, PC-3 cells of 48-h nocodazole treatment were morphologically large and multinucleated, consistent with 8N DNA content.

Figure 4C shows a bar graph comparing percentages of sub-G_1 populations (<2N) of the DNA content change in HeLa and PC-3 cells, in which the percentages of sub-G_1 cells were derived from flow cytometry analyses. The higher sub-G_1 phase cell accumulation in the HeLa population indicated that after completing mitotic arrest (48 h) with continuous nocodazole treatment, cells progressed to apoptosis and death (28). Those PC-3 cells showed no or less sub-G_1 cell peak after nocodazole treatment. Figure 4D shows a bar graph depicting the percentage of DNA ploidy change with 8N (may be due to G_2 arrest) only in PC-3 cells with nocodazole treatment, indicating that the hyperphosphorylation of Bub1 may account for aneuploidy formation due to incomplete mitotic arrest and endoreduplication.

Small Interfering RNA–Mediated Repression of Bub1 Restrains Cell Proliferation and Promotes Early Exit from Mitotic Checkpoint Arrest and Cytokinesis

To determine whether knockdown of Bub1 up-regulation or elimination of Bub1 hyperphosphorylation can stop the mitotic arrest delay and attenuate chromosomal overproliferation, we did small interfering RNA (siRNA) transfection experiments on *Bub1* gene expression (Figs. 4B and 5A). Synchronously growing PC-3 cells treated with nocodazole (0.2 μg/mL) were transfected with agent (control) and siRNA oligonucleotides (shown by different dozes at 30-90 pmol/mL). As shown in

Fig. 5A, protein levels of Bub1 were significantly reduced in siRNA transfectant cells against Bub1. By immunohistochemical analysis of the transfectant PC-3 and HeLa cells, positive immunohistochemical signals of Bub1 were noted to be significantly reduced in Bub1 knockdown cells as compared with transfection agent-only control (Fig. 5B). Bub1 staining was found only in the nucleus of mitotic cells, whereas there was no change of immunohistochemical staining in cytoplasm between knockdown and control cells. Knockdown of Bub1 cells did not display discernible growth defects.

We analyzed by flow cytometry the DNA content of siRNA transfectant cells. As shown in Fig. 5C, as compared with control (agent treatment only), a larger portion of cells with Bub1 RNA interference cells exited from mitotic arrest 24 h after treatment, resulting in an increased number of G_1 cells and decreased G_2-M cells (Fig. 5C). The number of 2N DNA (G_0-G_1 cells)–containing cells reached 36.8%, whereas the number of control cells was 12.5%, indicating active cytokinesis; in the control PC-3 cell group, 4N DNA content remained high, indicating persistent chromosomal over-endoreduplication. Forty-eight hours after treatment, with levels of Bub1 reduced, the levels of BubR1 were examined and the overall BubR1 levels were found to be apparently unchanged (Fig. 3A), indicating specificity of Bub1 siRNA knockdown. However, the level of phosphorylated BubR1 decreased (data not shown).

Inhibition of MAPK Activity Mimics Effects of Bub1 Depletion (siRNA) Experiments

Because MAPK was reported to be a key upstream activator of Bub1 phosphorylation (29, 30), we studied the effect of the MAPK inhibitor U0126 on PC-3 synchronously growing cell culture. Figure 5D shows the results of Western blotting experiment that MAPK inhibitor stopped Bub1 phosphorylation 40 h after nocodazole treatment in PC-3 cell cultures with double thymidine pretreatment synchronously at the G_1-S boundary. Phosphorylation of BubR1 was also significantly inhibited (Fig. 5D). Consistent with Western blotting, flow cytometry analysis of the DNA content in PC-3 cells showed inhibition by MAPK inhibitor U0126 (as shown in Fig. 5E); cytokinesis was initiated by a 2N peak 40 h after nocodazole treatment. As compared with siRNA-transfected PC-3 cells (Fig. 5C), MAPK inhibitor treatment resulted in a similar effect, but with a large portion of 2N cells exiting from mitotic arrest and entering cytokinesis.

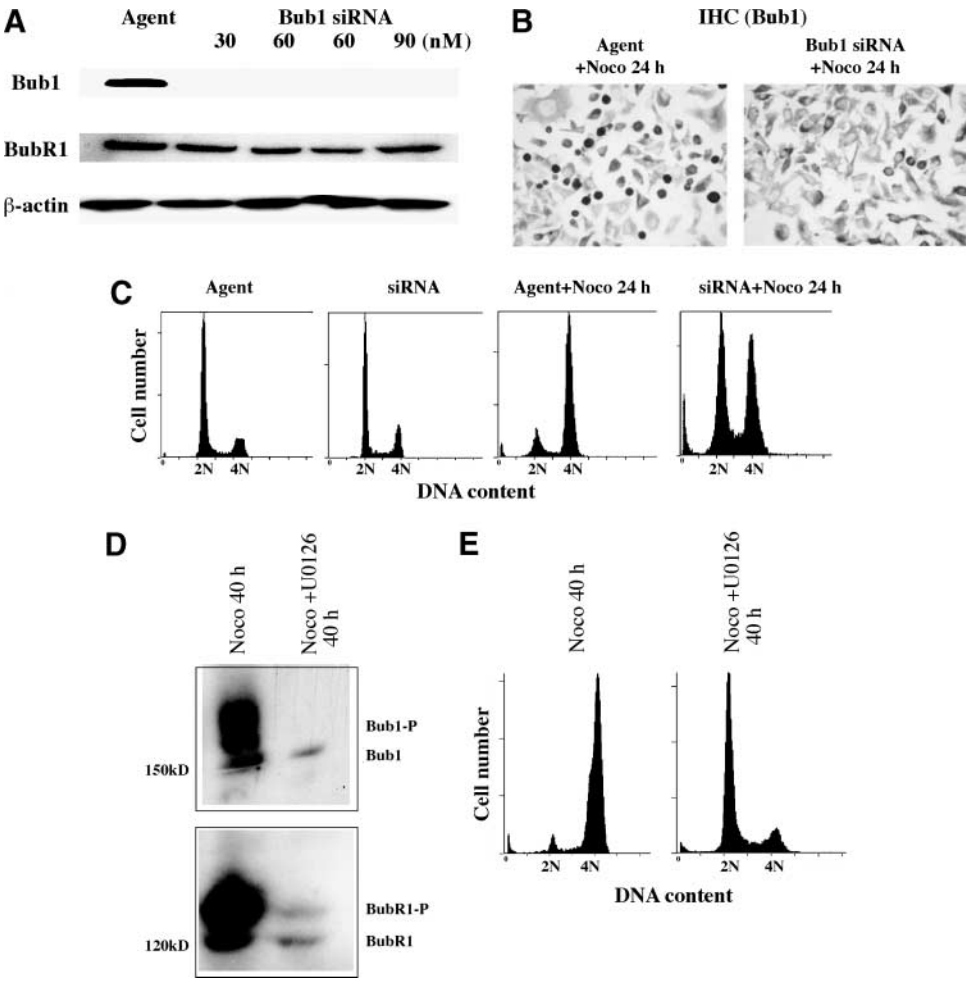

FIGURE 5. Knockdown of *Bub1* gene expression by siRNA (**A-C**) and inhibition of phosphorylation of Bub1 by MAPK inhibitor U0126 in PC-3 cells (**D-E**). **A.** Western blot analysis of the inhibition of Bub1 and BubR1 protein in the synchronously growing PC-3 cells transfected with different amounts (30, 60, 60, and 90 nmol/L) of siRNA. Control cells were treated with transfection agents only. Equal loading was confirmed by immunoblotting of β-actin. **B.** Immunohistochemical (*IHC*) analysis of the expression of Bub1 in the control (*Agent*) and knockdown (*Bub1 siRNA*) cells 24 h after treatment with 0.2 μg/mL nocodazole (*Noco*). **C.** Flow cytometry (DNA content) analysis of PC-3 cells of the control and Bub1 siRNA knockdown cells 24 h after nocodazole treatment. **D.** Western blotting (6% SDS-PAGE) experiment of MAPK inhibitor (U0126) in synchronously growing PC-3 cells. Cells were treated with 50 μmol/L of the MAPK/extracellular signal–regulated kinase kinase 1/2 inhibitor U0126 for 1 h, and then nocodazole (0.2 μg/mL) was added for 40 h. Blank control cell was treated only with dissolving reagents of U0126. **E.** Flow cytometry analysis of cells harvested for Western blot analysis (as in **D**).

Discussion

We have characterized a new feature in SV40 Tag oncogene–induced transgenic prostate cancer mouse models: *Bub1* gene up-regulation and protein hyperphosphorylation promote malignant transformation in SV40 Tag–induced transgenic mouse models. *Bub1* gene plays a unique and important role in tumorigenesis (mouse premalignant transformation prostatic intraepithelial neoplasia and microinvasion) and prostate cancer progression (androgen-independent and development of neuroendocrine carcinoma). This finding was achieved by a series of systematic chip array studies by taking advantage of a new knock-in mouse model, which features very synchronous tumor incidence and growth rate in the majority of well-differentiated to moderately differentiated prostate cancer. This led to the discovery that chromosomal instability, including genes related to DNA repair, replication, and spindle checkpoint systems, is a major feature of SV40 Tag oncogene–induced mouse models (Table 1). The new mechanism has been confirmed in our mouse prostate cancer model of rapidly growing PSP-TGMAP (similar to the TRAMP). Because of similarities of our two *in vivo* models with three well-established human prostate cancer cell lines, we extended our studies to cell culture and disclosed that the aneuploidy changes of the prostate cancer chromosomal structure are at least partly due to the impaired mitotic checkpoint function.

We underscore the important role that the *Bub1* gene plays in SV40 Tag–induced mouse transgenic prostate cancer models, which supports the recent report (9) that Bub1 is a SV40 Tag targeting protein. Furthermore, there is additional evidence: (*a*) As shown in our series of systematic chip assays, *Bub1* gene is most significantly up-regulated in all SV40 Tag binding/interaction (direct or indirect) proteins (Supplementary Table S2). (*b*) In our series cDNA microarray analyses (Table 1), *Bub1* is the only gene identified in all checkpoint-related genes to be up-regulated in both early-stage (slow-growing prostate cancer, with well-differentiated to moderately differentiated prostate cancers as in the PSP-KIMAP model) and rapidly growing prostate cancer (with poorly differentiated androgen-independent and neuroendocrine features, as in the TRAMP, LADY, and PSP-TGMAP models) models. (*c*) We showed *Bub1* gene overexpression to be associated with overexpression of Bub1 protein as a form of hyperphosphorylation in SV40-derived transgenic prostate cancer mouse models and also in human prostate cancer cell cultures, which may account for the impaired mitotic checkpoint system and chromosome aneuploid structure. *Bub1* gene up-regulation and protein hyperphosphorylation were higher in TGMAP mice (with advanced prostate cancer and higher aneuploidy) and in human prostate cancer cell lines (similar to TGMAP) than in KIMAP mice (well-differentiated to moderately differentiated cancer, mostly diploid tumor). (*d*) None of the androgen-independent or neuroendocrine-related genes listed in Table 1 were up-regulated genes related to SV40 Tag–induced tumorigenesis and early tumor progression, indicating androgen-independent or neuroendocrine development only represents the late stage of SV40 Tag–derived transgenic prostate cancer development (in TGMAP) as we previously reported (24).

Our observations suggest that the SV40 Tag oncoprotein promotes chromosomal instability and aneuploidy and the whole process of tumorigenesis and progression is possibly through perturbation of Bub1 function. It remains unclear whether in prostate tissue this is a specific effect of SV40 Tag on the *Bub1* gene or a multistep reaction (negative or positive feedback) of all SV40 Tag interaction proteins.

The mitotic checkpoint serves as a surveillance mechanism that ensures the faithful transmission of chromosomes from a mother cell to its two daughter cells during mitosis. Activation of the checkpoint involves kinetochore localization of several spindle checkpoint proteins, including Bub1, BubR1 (Mad3 in yeast), Bub3, MAPK, Mad1, Mad2, and Mps1 (reviewed in refs. 31-35). Phosphorylation is reportedly associated with mitotic checkpoint activation. Hyperphosphorylated components of the checkpoint machinery, including Bub1, BubR1, Bub3, Mad1, Mad2, Msp1, and Cenp-E, are associated with unattached kinetochores (29, 30, 36, 37). A recent study (18) proposed that defects in the mitotic checkpoint generate aneuploidy and might facilitate tumorigenesis. Aneuploidy contributes to, or even drives, tumor development.

We do not exclude the possibility that down-regulation of *Bub1* gene expression may also be the cause of cancer. However, deletion of checkpoint components (Bub1 and BubR1) normally result in early development defects (31), including megakaryopoiesis (38). The BubR1 insufficiency affects life span, aging-related aneuploidy, and senescence (39). Mutations of Bub1 and BubR1, along with several mitotic checkpoint genes, were rarely reported clinically (31, 40, 41). Up-regulation of checkpoint genes *Bub1* and *BubR1* was reported in several clinical studies on gastric (40) and colorectal malignancies with significantly shorter relapse-free survival rate (12).

It is noteworthy that that the most effectively up-regulated gene among all potential SV40 Tag interaction/targeting proteins in our studies was *Bub1*, a newly identified SV40 Tag targeting protein (for review, see refs. 10, 42). We assume that this maybe due to the use of the prostate tissue–specific promoters in transgenic mouse prostate cancer models, and also the strong promoters used for enhanced SV40 Tag expression. This may represent a prostate tissue–specific feature of SV40 Tag driven tumorigenesis and tumor progression in transformed cancer models. Current mouse transgenic prostate cancer models, including the most widely used TRAMP model, are all SV40 Tag oncogene derived, are all highly prostate tissue specific, and use very strong promoters. In our PSP94-derived SV40 Tag models, *PSP94* gene can drive 0.5 to 1 mg /mL protein expression in prostate secretory fluid, and rat probasin is at least as strong as PSP94 (43). There have been different reports in different tissues and models showing different mechanisms of the SV40 Tag oncogene–induced cancer development. Examples include mouse pancreatic islet carcinoma (14); neoplastic transformation of murine fibroblasts through signal transducer and activator of transcription-3 (14), p130-E2F/p107-E2F (13), and *VEGF* (17) gene up-regulation as SV40 Tag targeting factors in gonadal and adrenal tumorigenesis (16); and mesothelial tumor by affecting telomerase activity (44).

Due to the enforced transgenic SV40 Tag and Bub1 (BubR1 also) gene expression, we assume that the constant and persistent hyperphosphorylation of Bub1 protein is associated

with this up-regulated gene expression and will at least enhance the Bub1 autophosphorylation (45). Furthermore, the up-regulation of Bub1 may also account for chromosomal overproliferation, which starts from prostatic intraepithelial neoplasia in the prostate epithelial cells. Both of these overexpression factors may account for the mechanism overriding the spindle checkpoint control (i.e., the resultant mitotic checkpoint delay and kinetochore malfunctioning and the relative lack of response to microtubule toxin nocodazole; Fig. 3C). Human prostate cancer cell line PC-3 constantly showed a lower mitotic index with nocodazole treatments (Fig. 3E), which was also similarly reported by a mitotic arrest failure as in lung cancer cell lines (27). We observed that in PC-3 cells, chromosomal endoreduplication and impaired spindle checkpoint function following exposure to spindle (polyploid 8N peak as shown by flow cytometry in Fig. 4B and D); suppression of apoptosis after longer duration of nocodazole treatment (Fig. 3D; see flow cytometry in Fig. 4A and C). Furthermore, analysis of human prostate cancer lines showed that siRNA-mediated repression of Bub1 in the human prostate cancer line PC-3 restrained cell proliferation, an effect mimicked by inhibition of MAPK, an upstream activator of Bub1; knockdown or depletion of Bub1 expression can stop the constant hyperphosphorylation, attenuate chromosome overproliferation, and promote the exit, although early or premature, or response to mitotic arrest and facilitate cytokinesis. It is obvious that siRNA and MAPK inhibitor cannot be so precisely and appropriately adjusted to rectify or cure the Bub1 overexpression mechanism in either transgenic prostate cancer or human prostate cancer cell lines. We failed in obtaining pSilencer-CMV directed stable transfectant short hairpin RNA with knockdown of Bub1 protein phenotype, which may indicate a more critical role for *Bub1* gene regulation in kinetochore function, and its role in the mitotic checkpoint system (29, 30, 36, 46).

Our results showed a specific feature in the current most widely used transgenic prostate cancer models such that up-regulated Bub1/BubR1 by transgene can initiate tumor development and progression. As with Bub1, *BubR1* gene expression was also up-regulated in our SV40 Tag–derived prostate cancer models (Table 1; Fig. 1); BubR1 was also hyperphosphorylated (Fig. 3C) simultaneously with Bub1 at unattached kinetochores. Activation of BubR1 was also similar to Bub1 being MAPK dependent and MAPK was shown to contribute to Bub1 phosphorylation, and both kinases are activated by unattached chromosomes (29, 30, 36, 47). Inhibiting MAPK or altering MAPK consensus sites in Bub1 abolished the phosphorylation (30). Because phosphorylation of BubR1 at kinetochores requires the Bub1 kinase activity, it is possible that Bub1 may directly or indirectly phosphorylate BubR1.

This is the first report on the role of the up-regulation of the *Bub1* gene and mitotic checkpoint system in SV40 Tag–derived prostate cancer models, and also the first analogous observation in human prostate cancer cell lines. A previous study in yeast did report similar results as in the transgenic prostate cancer models that up-regulation of *Bub1* gene caused a mitotic arrest delay (48). Overexpression of a kinetochore related gene, *Pim* (also listed in Table 1), in prostate cancer cell lines led to overriding of mitotic spindle checkpoint and genomic instability (49). The finding of the new mechanism in SV40 Tag–derived mouse prostate cancer models is significant, especially the key role that the *Bub1* gene plays in early tumorigenesis and progression, because it will provide a novel direction and a new field for research on new therapeutic targets in the prevention and intervention of prostate cancer.

Materials and Methods

Genetically Engineered Murine Models of PSP-TGMAP (Transgenic Mouse Adenocarcinoma Prostate) and PSP-KIMAP (Knock-in Mouse Adenocarcinoma Prostate) Models

Transgenic (TGMAP; refs. 4, 5) and knock-in (KIMAP; refs. 23, 24) SV40 Tag models were reported previously. Both models used a prostate tissue–specific gene, the mouse PSP94 promoter/enhancer region (3,842 bp). The resulting TGMAP model developed large, visible tumors (~2 cm) at 6 months (26-28 weeks) of age, with lymph node metastases. The KIMAP model established (23) was characterized by a steady and synchronous tumor growth kinetics, whereby only at the very later stage (>70 weeks) were nonsynchronous tumors found (23-25). This feature is similar to that of late-stage prostate cancer mice in the TGMAP model. Transgenic mice were identified by a quick PCR genotyping protocol (4, 23). All animal experiments were conducted according to standard protocols approved by the University of Western Ontario Council on Animal Care. Procedures of genotyping, transgenic and knock-in mice breeding, anatomic dissection, and pathologic and histologic grading were all done as previously reported (4, 5, 23, 24).

cDNA Microarray Analysis

cDNA microarray analysis was done on prostate tumor tissues (ventral and dorsolateral lobes) from KIMAP mice from two age groups: 20 weeks (n = 7) and 60 weeks (n = 10). Prostate tissues from wild-type mice (n = 7-12; 50-100 mg each) were pooled and total RNA used as a control. For comparison, PSP-TGMAP (6 months with large-sized palpable prostate cancer) and KIMAP (52-70 weeks; n = 12 mice) were used. Total cellular RNA from prostate tumors dissected was first isolated with TriZol (Invitrogen, Carlsbad, CA) and then further purified using the RNeasy Mini Kit (Qiagen, Valencia, CA). RNA samples from single mouse prostate tissue were individually characterized with an Agilent 2100 Bioanalyzer (Agilent, Palo Alto, CA) separately. Only pooled RNA samples were used because the amount of a single mouse prostate tissue was insufficient for both pathohistologic/slide study and RNA sample preparation. All chip experiments were done at the London Regional Genomics Centre (London, Ontario, Canada) as we previously reported (24). cDNA and cRNA syntheses were done as per GeneChip Expression Analysis Technical Manual protocols (Affymetrix, Santa Clara, CA). The quality of the labeled target was assessed on a Test 3 array before hybridization to the MOE430A GeneChip (for KIMAP mice, 45,000 probe sets, for >39,000 transcripts and variants from >34,000 well-characterized mouse genes sized *in situ* on the array). For cDNA microarray comparing TGMAP (n = 12) and

KIMAP (n = 12) mice, an MG_U74Av2 GeneChip was used, which contains ~12,000 probe sets composed of ~6,000 mouse genes and 6,000 estimated sequence transcripts.

Analysis of results was conducted on single array and comparison array. Gene expression levels of samples were normalized and analyzed using Microarray Suite, MicroDB 3.0 software (Affymetrix). Using MicroDB 3.0 and Data Mining Tool 3.0, genes showing altered expression were identified and subjected to further analysis using programs in the public domain.[7] Classification was determined by National Center for Biotechnology Information/Unigene and PubMed publications.

Semiquantitative RT-PCR

The human *Bub1* and *BubR1* genes, mouse *Bub1* and *BubR1*, and internal control *GAPDH* (human and mouse) were analyzed using semiquantitative RT-PCR. RNA was isolated from prostate tissues and human prostate cancer cell lines: LNCaP (wild-type p53, androgen responsive, androgen dependent), DU145 (androgen independent), and PC-3 (androgen independent) using a TRI-reagent according to the manufacturer's instructions. Total RNA fractionations of cytoplasmic and nuclear RNA were prepared as previously reported (50). The RNA template was reverse transcribed into cDNA for 50 min at 37°C. PCR reaction program comprises cycles of 94°C, 30 s; 60°C, 30 s; and 72°C, 60 s, and final extension for 10 min at 72°C. To compare PCR products semiquantitatively, 20 to 35 cycles of PCR (extension temperature 72°C) were done to determine the linearity of the PCR amplification, and the amplified *GAPDH* cDNA served as an internal control for cDNA quantity and quality. All RNA samples were treated with DNase I to avoid genomic DNA contaminations. Oligonucleotide primer pairs used for PCR are human Bub1 (forward, 5′-CACGATCCCTATGATTGTAAC-3′; reverse, 5′-GGTAGTGCATCTAAATGTGTC-3′), human BubR1 (forward, 5′-CTCAGCAACAAACCATGGAAC-3′; reverse, 5′-CTATTACGTAGGGCCCTAATC-3′), mouse Bub1 (forward, 5′-TGTCCTGAGATGCTCAGTAAC-3′; reverse, 5′-AGTGTGTTTTGGAGAAGGTCC-3′), mouse BubR1 (forward, 5′-CTAGCGCACTTACTCCTGTTC-3′; reverse, 5′-CTGATGTGTCTAAGTGTGCTC-3′), and control gene *GAPDH* (forward, 5 ′-CCACCTTCTTGATGTCATCA-3′; reverse, 5′-TATTGGGCGCCTGGTCACCA-3′). Amplified PCR products were visualized on a 2% agarose gel. Amplification yielded the predicted size of the respective amplified fragments.

Cell Culture, Synchronization, and Cell Cycle Analysis

Three human prostate carcinoma cell lines differing in androgen dependency, LNCaP (androgen dependent), DU145 (androgen independent), and PC-3 (androgen independent), were maintained in RPMI 1640 (DMEM; Invitrogen/Life Technologies, Carlsbad, CA) supplemented with 10% fetal bovine serum. All cells were maintained at standard cell culture conditions (37°C, 5% CO_2 in a humidified incubator).

To generate synchronized populations, prostate tumor PC-3 cells were arrested at the G_1-S boundary by a double thymidine block (procedures named "T minus S" and "G_2 + mitosis + G_1") as previously described (46), with modifications. Human cervical tumor HeLa cells were used as control. In brief, 5×10^5 HeLa and PC-3 cells were plated onto 25-cm^2 flasks and treated with the first thymidine block (2 mmol/L) at the G_1-S boundary for 14 h; excess thymidine (2 mmol/L) was added for the inhibition of dCDP formation from CDP, leading to inhibition of DNA replication and arrest of the cell cycle in S phase. After the first treatment, cells were washed and cultivated with fresh medium free of thymidine for 8 h, then the cells were treated with second thymidine block for another 14 h for synchronous growth passing G_2 + mitosis + G_1. Cells were released into fresh medium for 4 h before adding nocodazole (0.2 μg/mL). At different time points, cells were harvested and fixed with 70% ethanol for further analysis.

For MAPK inhibition experiment, synchronous cells were treated with 50 μmol/L of the MAPK/extracellular signal–regulated kinase kinase 1/2 inhibitor U0126 [1,4-diamino-2,3-dicyano-1,4-bis (2-aminophenylthio) butadiene; Sigma-Aldrich, St. Louis, MO; ref. 51] for 1 h, and then nocodazole (0.2 μg/mL) was added for 40 h. Control cells were treated only with the same concentration of DMSO (U0126-dissolving reagents) as U0126 treatment cells.

Flow Cytometry

Flow cytometric analysis of DNA content was done in prostate malignant tissues obtained from both TGMAP and KIMAP models (n = 8 each), either freshly excised or liquid nitrogen snap frozen. Preparation of single-cell suspension was done according to the standard clinical procedures in our Hospital. Before analysis, the cell suspension was filtered through a nylon mesh to remove any debris and cell aggregates. To establish the normal diploid DNA peak position, normal mouse spleen lymphocytes were dissociated and used as a control. For flow cytometry in tissue culture, 1×10^4 to 2×10^4 cells were harvested at different time points and peripheral blood leukocytes were isolated as controls using Ficoll-Paque Plus (Amersham-Pharmacia, Montreal, Quebec, Canada) from human blood. All samples were analyzed with the EPICS C flow cytometer (Coulter Electronics, Hialeah, FL). The resultant single nuclei suspension was treated with ribonuclease and stained with 50 μg/mL propidium iodide (Beckman Coulter, Inc., Miami, FL). DNA histograms were classified as diploid, tetraploid, or aneuploid. DNA aneuploidy was defined by the presence of a tumor population with a definable G_0-G_1 peak, which was distinct from the diploid population. Tetraploidy (4N) was defined by a peak with a DNA index (ratio of the channel number of the abnormal to the diploid population) of between 1.9 and 2.1. DNA proliferation rate was measured by flow cytometry as values of %S (percent S-phase) and %S + %G_2-M (percent S-phase and G_2-M phase) separately. The sub-G_1 phase cells (<2N) were calculated for characterizing apoptosis and death as per Shin et al. (28).

Mitotic Index Analysis

For determination of mitotic index (proportion of cells in mitosis), synchronized cells were treated with 0.2 μg/mL nocodazole at various time points; cells were harvested and fixed in 4% paraformaldehyde for 30 min. Mitotic cells were identified based on appearance of condensed nuclear chromatin

[7] http://www.affymetrix.com/analysis/go.

by staining with 4′,6-diamidino-2-phenylindole (0.1 μg/mL; Sigma-Aldrich) according to ref. 27. At least 300 cells in each of three independent experiments were counted for each time point by fluorescence microscopy. Cells having condensed chromosomes without a nuclear membrane were regarded as mitotic cells.

Western Blotting and Immunohistochemistry

Antibodies used in this study were as follows: antihuman Bub1, antihuman BubR1 (polyclonal, 1:1,000; from Dr. S.S. Taylor; refs. 36, 46), antimouse Bub1 (monoclonal, 1:1,000; Chemicon, Temecula, CA), and anti-β-actin (polyclonal, 1:2,000; Sigma). Standard SDS-PAGE and Western blotting procedures were followed as previously reported (4, 5). Briefly, PC-3 and HeLa cells and tissues were lysed in lysis buffer [50 mmol/L Tris/HCl (pH 7.8), 150 mmol/L NaCl, 1.0% Triton X-100, 1 mmol/L EDTA, 1 mmol/L EGTA, 1 mmol/L phenylmethylsulfonyl fluoride, 2 mmol/L Na_3VO_4, 10 mmol/L, β-glycerophosphate, 5 mmol/L Nappi (sodium pyrophosphate)] according to refs. 45, 46. The cells were then scraped and the suspension (cells with lysis buffer) was transferred into a centrifuge tube and kept on ice for 20 min with occasional inversion to ensure complete cell lysis. The cell suspension was cleared by centrifugation at 14,000 × *g* for 15 min at 4°C, and the supernatant (total cell lysate) was either used immediately or stored at −80°C. Protein concentrations were determined using the DC Protein Assay (Bio-Rad Laboratories, Hercules, CA) as per manufacturer's protocol. Sixty micrograms of total proteins were separated by SDS-PAGE, followed by transfer to a polyvinylidene difluoride membrane (Roche, Laval, CA), and immunoblotted with the indicated antibody followed by an appropriate horseradish peroxidase–conjugated secondary antibody. The membrane was detected with a freshly prepared chemiluminescent solution [100 mmol/L Tris-HCl (pH 8.5), 0.018% H_2O_2 (v/v), 1.25 mmol/L Luminol, 225 nmol/L coumaric acid].

Depletion of Bub1 by siRNA

The siRNA used in this study was synthesized by Ambion (Austin, TX). The target sequence is exon 25 of Bub1 in the encoding protein kinase region (National Center for Biotechnology Information accession no. NM_004336). The PC-3 cells were plated in six-well plates at 2.5×10^4 per well. Cells were treated with thymidine for synchronized growth. Cells were transfected with 60 nmol/L Bub1 siRNA or nonsense siRNA using an amine reagent (SiPORTAmine, Ambion) as described by the manufacturer. Twenty four hours before harvest, cells were treated with the spindle-damaging toxin nocodazole (0.2 μg/mL). Cells were tested for protein levels of Bub1 by Western blotting and for DNA content by flow cytometry.

Acknowledgments

We thank Dr. Hongtao Yu for critical reading of the manuscript and the University of Western Ontario Transgenic and Gene Targeting Facility.

References

1. Abate-Shen C, Shen MM. Mouse models of prostate carcinogenesis. Trends Genet 2002;18:S1–5.

2. Huss WJ, Maddison LA, Greenberg NM. Autochthonous mouse models for prostate cancer: past, present and future. Semin Cancer Biol 2001;11:245–60.

3. Greenberg NM, Demayo F, Finegold MJ, et al. Prostate cancer in a transgenic mouse. Proc Natl Acad Sci U S A 1995;92:3439–43.

4. Gabril MY, Onita T, Ji PG, et al. Prostate targeting: PSP94 gene promoter/enhancer region directed prostate tissue-specific expression in a transgenic mouse prostate cancer model. Gene Ther 2002;9:1589–99.

5. Wirtzfeld LA, Wu GJ, Bygrave M, et al. Three-dimensional ultrasound microimaging for preclinical studies using a transgenic prostate cancer mouse model. Cancer Res 2005;65:6337–45.

6. Masumori N, Thomas TZ, Chaurand P, et al. A probasin-large T antigen transgenic mouse line develops prostate adenocarcinoma and neuroendocrine carcinoma with metastatic potential. Cancer Res 2001;61:2239–49.

7. Winter SF, Cooper AB, Greenberg NM. Models of metastatic prostate cancer: a transgenic perspective. Prostate Cancer Prostatic Dis 2003;6:204–11.

8. Shappell SB, Thomas GV, Roberts RL, et al. Prostate pathology of genetically engineered mice: definitions and classification. The consensus report from the Bar Harbor meeting of the Mouse Models of Human Cancer Consortium Prostate Pathology Committee. Cancer Res 2004;64:2270–305.

9. Cotsiki M, Lock RL, Cheng Y, et al. Simian virus 40 large T antigen targets the spindle assembly checkpoint protein Bub1. Proc Natl Acad Sci U S A 2004;101:947–52.

10. Sullivan CS, Pipas JM. T antigens of simian virus 40: molecular chaperones for viral replication and tumorigenesis. Microbiol Mol Biol Rev 2002;66:179–202.

11. Ali SH, DeCaprio JA. Cellular transformation by SV40 large T antigen: interaction with host proteins. Semin Cancer Biol 2001;11:15–22.

12. Shichiri M, Yoshinaga K, Hisatomi H, Sugihara K, Hirata Y. Genetic and epigenetic inactivation of mitotic checkpoint HBUB1 and HBUBR1 and their relationship to survival. Cancer Res 2002;62:13–7.

13. Sullivan CS, Baker AE, Pipas JM. Simian virus 40 infection disrupts p130-2F and p107-2F complexes but does not perturb pRb-E2F complexes. Virology 2004;320:218–28.

14. Vultur A, Arulanandam R, Turkson J, Niu G, Jove R, Raptis L. Stat3 is required for full neoplastic transformation by the Simian Virus 40 large tumor antigen. Mol Biol Cell 2005;16:3832–46.

15. Hager JH, Hodgson JG, Fridlyand J, Hariono S, Gray JW, Hanahan D. Oncogene expression and genetic background influence the frequency of DNA copy number abnormalities in mouse pancreatic islet cell carcinomas. Cancer Res 2004;64:2406–10.

16. Mikola M, Kero J, Nilson JH, Keri RA, Poutanen M, Huhtaniemi I. High levels of luteinizing hormone analog stimulate gonadal and adrenal tumorigenesis in mice transgenic for the mouse inhibin-α-subunit promoter/Simian virus 40 T-antigen fusion gene. Oncogene 2003;22:3269–78.

17. Catalano A, Romano M, Martinotti S, Procopio A. Enhanced expression of vascular endothelial growth factor (VEGF) plays a critical role in the tumor progression potential induced by simian virus 40 large T antigen. Oncogene 2002;21:2896–900.

18. Kops GJ, Weaver BA, Cleveland DW. On the road to cancer: aneuploidy and the mitotic checkpoint. Nat Rev Cancer 2005;5:773–85.

19. Dube JY, Frenette G, Paquin R, et al. Isolation from human seminal plasma of an abundant 16-kDa protein originating from the prostate, its identification with a 94-residue peptide originally described as β-inhibin. J Androl 1987;8:182–9.

20. Abrahamsson P-A, Lilja H, Falkmer S, Wadstrom LB. Immunohistochemical distribution of the three predominant secretory proteins in the parenchyma of hyperplastic and neoplastic prostate glands. Prostate 1988;12:39–46.

21. Weiber H, Anderson C, Murne A, et al. β-microseminoprotein is not a prostate-specific protein. Am J Pathol 1990;137:593–603.

22. Fernlund P, Granberg L, Larson I. Cloning of b-microseminoprotein of the rat: a rapidly evolving mucosal surface protein. Arch Biochem Biophys 1996;334:73–82.

23. Duan WM, Gabril MY, Moussa M, et al. Knock-in of SV40 Tag oncogene in a mouse adenocarcinoma of the prostate (KIMAP) model demonstrates advantageous features over the transgenic model. Oncogene 2005;24:1510–24.

24. Gabril MY, Duan WM, Wu GJ, et al. A novel knock-in prostate cancer model demonstrates biology similar to that of human prostate cancer and suitable for preclinical studies. Mol Ther 2005;11:348–62.

25. Van Huizen I, Wu GJ, Moussa M, et al. Establishment of a serum tumor marker for pre-clinical trials of mouse prostate cancer models. Clin Cancer Res 2005;11:7911–9.

26. So WJ, Cheville JC, Katzmann JA, et al. Factors that influence the measurement of prostate cancer DNA ploidy and proliferation in paraffin embedded tissue evaluated by flow cytometry. Mod Pathol 2001;14:906–12.

27. Masuda A, Maeno K, Nakagawa T, Saito H, Takahashi T. Association between mitotic spindle checkpoint impairment and susceptibility to the induction of apoptosis by anti-microtubule agents in human lung cancers. Am J Pathol 2003;163:1109–16.

28. Shin HJ, Baek KH, Jeon AH, et al. Dual roles of human BubR1, a mitotic checkpoint kinase, in the monitoring of chromosomal instability. Cancer Cell 2003;4:483–97.

29. Chen RH. BubR1 is essential for kinetochore localization of other spindle checkpoint proteins and its phosphorylation requires Mad1. J Cell Biol 2002;158: 487–96.

30. Chen RH. Phosphorylation and activation of Bub1 on unattached chromosomes facilitate the spindle checkpoint. EMBO J 2004;23:3113–21.

31. Bharadwaj R, Yu H. The spindle checkpoint, aneuploidy, and cancer. Oncogene 2004;23:2016–27.

32. Margolis RL. Bub1, a gatekeeper for Cdc20-dependent mitotic exit. Dev Cell 2004;7:634–5.

33. Tang Z, Shu H, Oncel D, Chen S, Yu H. Phosphorylation of Cdc20 by Bub1 provides a catalytic mechanism for APC/C inhibition by the spindle checkpoint. Mol Cell 2004;16:387–97.

34. Chan GK, Yen TJ. The mitotci checkpoint: a signaling pathway that allows a single unattached kinetochore to inhibit mitotic exit. Prog Cell Cycle Res 2003;5: 431–9.

35. Grady WM. Genomic instability and colon cancer. Cancer Metastasis Rev 2004;23:11–27.

36. Taylor SS, Hussein D, Wang Y, Elderkin S, Morrow CJ. Kinetochore localisation and phosphorylation of the mitotic checkpoint components Bub1 and BubR1 are differentially regulated by spindle events in human cells. J Cell Sci 2001;114:4385–95.

37. Li W, Lan Z, Wu H, et al. BUBR1 phosphorylation is regulated during mitotic checkpoint activation. Cell Growth Differ 1999;10:769–75.

38. Wang Q, Liu T, Fang Y, et al. BubR1 deficiency results in abnormal megakaryopoiesis. Blood 2005;103:1278–85.

39. Baker DJ, Jeganathan KB, Cameron JD, et al. BubR1 insufficiency causes early onset of aging-asociated phenotypes and infertility in mice. Nat Genet 2004; 36:744–9.

40. Grabsch H, Takeno S, Parsons WJ, et al. Overexpression of the mitotic checkpoint genes BUB1, BUBR1, and BUB3 in gastric cancer—association with tumour cell proliferation. J Pathol 2003;200:16–22.

41. Grabsch HI, Askham JM, Morrison EE, et al. Expression of BUB1 protein in gastric cancer correlates with the histological subtype, but not with DNA ploidy or microsatellite instability. J Pathol 2004;202:208–14.

42. Sullivan CS, Tremblay JD, Fewell SW, Lewis JA, Brodsky JL, Pipas JM. Species-specific elements in the large T-antigen J domain are required for cellular transformation and DNA replication by simian virus 40. Mol Cell Biol 2000;20: 5749–57.

43. Imasato Y, Onita T, Moussa M, et al. Rodent PSP94 gene expression is more specific to the dorsolateral prostate and less sensitive to androgen ablation than probasin. Endocrinol 2001;142:2138–46.

44. Foddis R, De Rienzo A, Broccoli D, et al. SV40 infection induces telomerase activity in human mesothelial cells. Oncogene 2002;21:1434–42.

45. Sharp-Baker H, Chen RH. Spindle checkpoint protein Bub1 is required for kinetochore localization of Mad1, Mad2, Bub3, and CENP-E, independently of its kinase activity. J Cell Biol 2001;153:1239–50.

46. Chan GK, Schaar BT, Yen TJ. Characterization of the kinetochore binding domain of CENP-E reveals interactions with the kinetochore proteins CENP-F and hBUBR1. J Cell Biol 1998;143:49–63.

47. Taylor SS, McKeon F. Kinetochore localization of murine Bub1 is required for normal mitotic timing and checkpoint response to spindle damage. Cell 1997; 89:727–35.

48. Farr KA, Hoyt MA. Bub1p kinase activates the *Saccharomyces cerevisiae* spindle assembly checkpoint. Mol Cell Biol 1998;18:2738–47.

49. Roh M, Gary B, Song C, et al. Overexpression of the oncogenic kinase pim-1 leads to genetic instability. Cancer Res 2003;63:8079–84.

50. Xuan JW, Chin JL, Guo Y, Chambers AF, Finkelman MA, Clarke MW. Alternative splicing of PSP94 (prostate secretory protein of 94 amino acids) mRNA in prostate tissue. Oncogene 1995;11:1041–7.

51. Beloueche-Babari M, Jackson LE, Al Saffar NM, Workman P, Leach MO, Ronen SM. Magnetic resonance spectroscopy monitoring of mitogen-activated protein kinase signaling inhibition. Cancer Res 2005;65:3356–63.

Molecular Cancer Research

Bub1 Up-Regulation and Hyperphosphorylation Promote Malignant Transformation in SV40 Tag–Induced Transgenic Mouse Models

Conghui Guo, Guojun Wu, Joseph L. Chin, et al.

Mol Cancer Res 2006;4:957-969.